Mathematical and Computational Applications

MDPI

Article

An Improved Approach Based on a New Laplace Model Using Classical and Risk Measures

Morad Alizadeh [1], Gauss M. Cordeiro [2], Jondeep Das [3,4], Partha Jyoti Hazarika [3], Javier E. Contreras-Reyes [5,6,*], Mohamed S. Hamed [7] and Haitham M. Yousof [8]

1 Department of Statistics, Faculty of Intelligent Systems Engineering and Data Sciences, Persian Gulf University, Bushehr 75169, Iran; moradalizadeh78@gmail.com
2 Department of Statistics, Federal University of Pernambuco, Recife 50670-901, Brazil; gauss@de.ufpe.br
3 Department of Statistics, Dibrugarh University, Dibrugarh 786004, India; jondeepdas98@gmail.com (J.D.); parthajhazarika@gmail.com (P.J.H.)
4 Department of Statistics, Bhattadev University, Assam 781325, India
5 Instituto de Matemática, Física y Estadística, Facultad de Ingeniería y Negocios, Universidad de Las Américas, Sede Viña del Mar, 7 Norte 1348, Vina del Mar 2531098, Chile
6 Centro de Modelación Ambiental y Dinámica de Sistemas (CEMADIS), Facultad de Ingeniería y Negocios, Universidad de Las Américas, Avenida Manuel Montt Nº 948, Santiago 7500975, Chile
7 Department of Business Administration, Gulf Colleges, Hafr Albatin 121235, Saudi Arabia; mmmansour@taibahu.edu.sa
8 Department of Statistics, Mathematics and Insurance, Faculty of Commerce, Benha University, Benha 13511, Egypt; haitham.yousof@fcom.bu.edu.eg
* Correspondence: jecontrr@uc.cl

Abstract

In this paper, we propose a generalized odd log-logistic standard Laplace model and study some of its main properties. The novelty of this model is based on classical and risk-based measures to effectively analyze the body mass index (BMI) data. The analysis underscores the importance of a multidisciplinary approach in addressing challenges related to health, performance, and risk management. The proposed methodology not only is helpful to understand the variability of BMI measurements, but also prove how common statistical models considered in financial field can be effectively adapted to other ones, offering insights that drive informed decision-making and strategic planning.

Keywords: BMI measurements; economic risk; maximum likelihood; Laplace distribution; skewness; tail behavior

Check for updates

Academic Editor: Sandra Ferreira

Received: 26 November 2025
Revised: 9 January 2026
Accepted: 13 January 2026
Published: 17 January 2026

Copyright: © 2026 by the authors. Licensee MDPI, Basel, Switzerland. This article is an open access article distributed under the terms and conditions of the Creative Commons Attribution (CC BY) license.

1. Introduction

The Laplace (La) distribution is used for symmetric data, just as the normal one. However, it is well-suited for symmetric data with extended tails, whereas the normal for symmetric data with short tails. The cumulative distribution function (CDF) of the standard La is

$$\Pi(x) = \begin{cases} 1 - 0.5e^{-x}, & x > 0, \\ 0.5e^{x}, & x \leq 0. \end{cases}$$

La distribution has continuously evolved since it started for several kinds of methodologies. In particular, the traditional La distribution behaves most effectively in symmetric scenarios. Based on the skew-normal (SN) [1,2] introduced an asymmetric adaptation of

La distribution to overcomes this drawback. The skew La (SLa) distribution is a good adaptation to handle asymmetric unimodal data.

On the other hand, body mass index (BMI) is a key indicator of overall physical condition and extreme values (either too high or too low), which are related to underlying health concerns, such as obesity, malnutrition, or increased susceptibility to chronic conditions such as cardiovascular disease. In addition, the La distribution is known for modeling heavy tails and particularly suited to analyze extreme BMI data that pose significant health risks. This makes it ideal for Value at Risk (VaR) analysis in health contexts. Athletes often have BMI distributions that differ from the general population due to muscle mass and training regimens. A specialized model tailored to this demographic, as discussed in the paper, would provide more meaningful and actionable insights for sports science and health management. The BMI data often show variability due to demographic and lifestyle factors. An extended La model could accommodate these variations more effectively than existing models. Extensions to La distribution contributes to the evolution of statistical methods, providing researchers with a more flexible tool that bridges gaps in current methodologies while offering enhanced analytical precision.

Unlike traditional methods such as VaR analysis, which rely on normal assumptions, this method has proved the effectiveness of La distribution for extreme events and stock market fluctuations. Based on an empirical analysis of housing data, the study underscores the ability of this distribution to forecast risk management and investment strategies. It aligns with a risk analysis, where significant advances have been made. Contributions from [3] on threshold effects, ref. [4] on tail risk premiums, and [5] on tail mean-variance offer nuanced perspectives on risk measures. Recent innovations include Bayesian risk frameworks [6], and loss probability models [7], reflecting a shift toward sophisticated techniques for assessing financial risks. These developments improve the precision of risk assessments, supporting more informed decisions by investors and policymakers. The improved La model would represent an innovative contribution to the field, particularly if it outperforms existing statistical methods in terms of accuracy and interpretability of BMI data. Our research would establish a new standard for BMI risk analysis. For more details, see [8,9].

Section 2 introduces a new extended La distribution based on the method outlined in [10]. Section 3 reports some structural properties. Section 4 deals with maximum likelihood estimation. Section 5 provides some simulations to examine the accuracy of the estimates. Section 6 addresses two real applications. Section 7 performs some hypothesis tests, and Section 8 considered some risk measures. Finally, Section 9 gives some conclusion remarks.

2. The Model

We define the "Generalized Odd Log-Logistic Standard Laplace" (GOLLSLa) distribution within the family introduced by [10], as follows.

Definition 1. *Henceforth, $X \sim GOLLSLa(a, b)$. The CDF of X is given by*

$$F(x) = \left[\Pi(x)^{ab} + \{1 - \Pi(x)^{a}\}^{b}\right]^{-1} \Pi(x)^{ab}, \tag{1}$$

where $a > 0$ and $b > 0$ are two parameters, and $\Pi(x)$ is the standard La CDF.

Definition 2. *The probability density function (PDF) of $X \sim GOLLSLa(a, b)$ has the form*

$$f(x) = a\, b\, \pi(x)\, \Pi(x)^{ab-1} [1 - \Pi(x)^{a}]^{b-1} \left\{\Pi(x)^{ab} + [1 - \Pi(x)^{a}]^{b}\right\}^{-2}, \tag{2}$$

where $\pi(x) = \frac{\mathrm{d}}{\mathrm{d}x}\Pi(x)$.

Proof. Equation (2) is straightforward from (1). □

Remark 1. *Some subclasses of GOLLSLa distribution are:*

i. *For* $a = 1$, $X \sim$ *odd log-logistic standard La (OLLSLa).*
ii. *For* $b = 1$, $X \sim$ *exponentiated standard La (ESLa).*
iii. *For* $a = b = 1$, $X \sim La$.

Figures 1 and 2 give the PDF and CDF of X for some parameters, respectively.

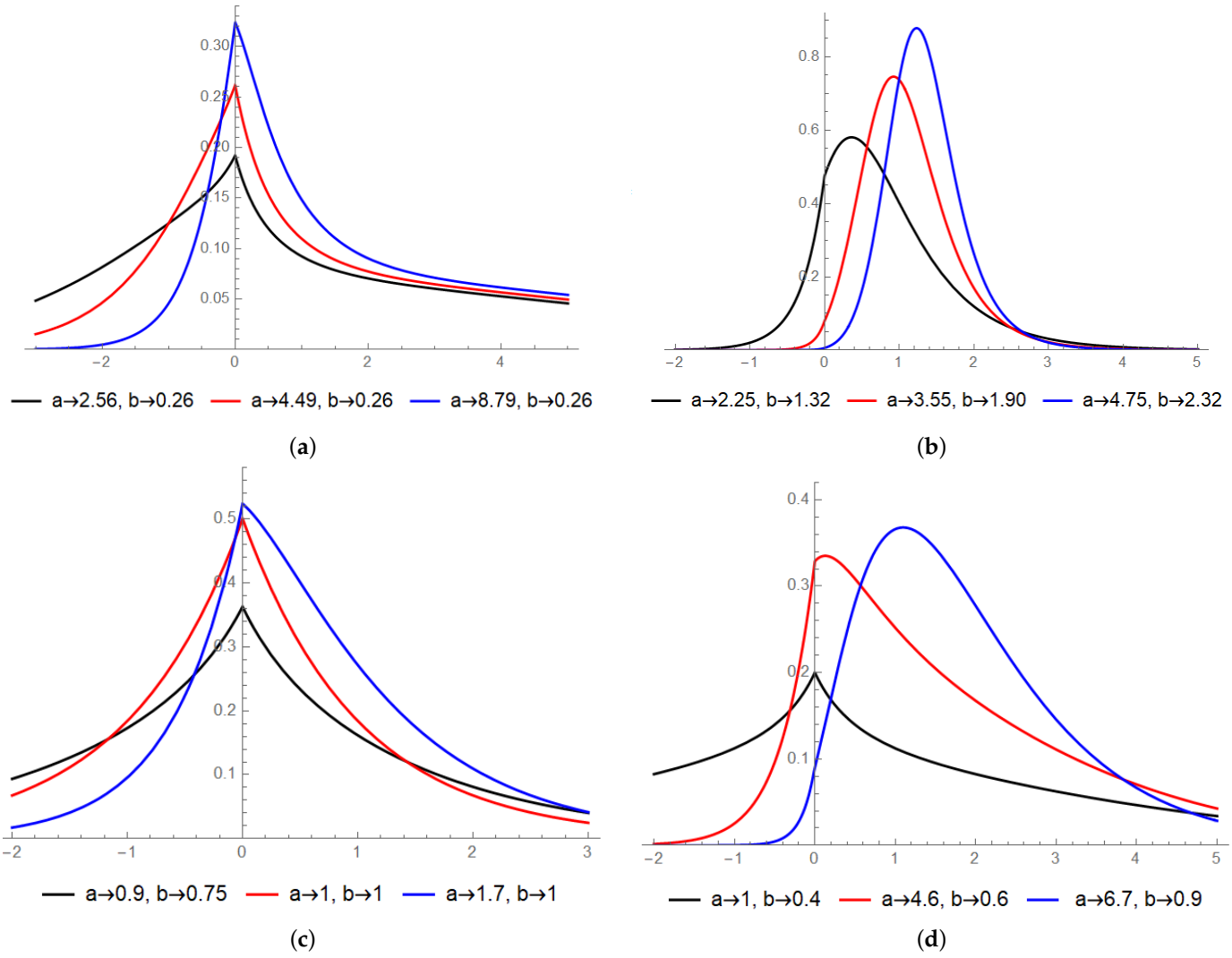

Figure 1. PDF of $X \sim \mathrm{GOLLSLa}(a, b)$ for several a and b parameters. (**a**) PDF with a large a and small b (fixed) to produce a sharp, highly concentrated peak. (**b**) PDF with larger a values (ranging from 2.25 to 4.75) and a small b (ranging from 1.32 to 2.32), demonstrating an increasingly concentrated and peaked shape as a grows. (**c**) PDF with small to moderate a values (0.9 to 1.7) paired with varying b values (0.75 to 1), showing how decreasing b can compress and elevate the mode dramatically. (**d**) PDF with $a = 1$ and a small $b = 0.4$ compared to cases with larger a (4.6, 6.7) and slightly larger b (0.6, 0.9), illustrating a transition from a very narrow peak to broader, more moderate concentrations.

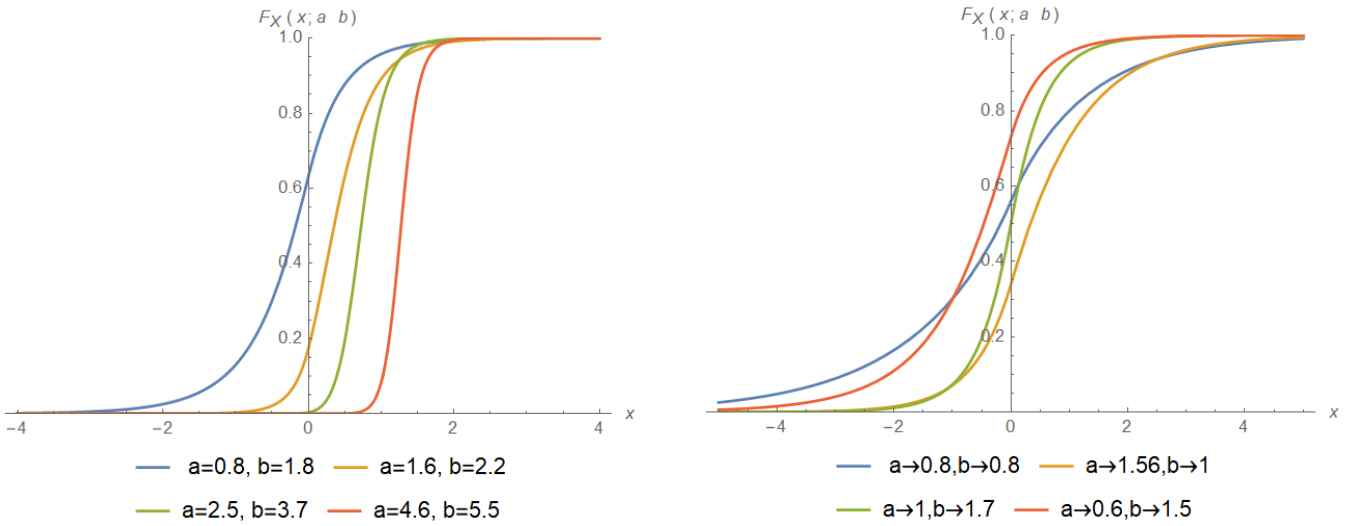

(**a**) (**b**)

Figure 2. CDF of $X \sim \text{GOLLSLa}(a, b)$ for several a and b parameters. (**a**) CDFs for increasing values of a and b, illustrating sharper transitions around the central region and faster convergence to one as both parameters increase. (**b**) CDFs for different combinations of small and moderate values of a and b, highlighting the flexibility of the model in controlling skewness and tail behavior, particularly around the origin and in the right tail.

3. Main Properties

3.1. Quantile Function

Let $u \sim U(0,1)$. If

$$\left(\frac{u^{1/b}}{u^{1/b}+(1-u)^{1/b}}\right)^{1/a} \leq \frac{1}{2},$$

then

$$X_u = \log\left[2\left(\frac{u^{1/b}}{u^{1/b}+(1-u)^{1/b}}\right)^{1/a}\right],$$

otherwise

$$X_u = -\log\left[2-2\left(\frac{u^{1/b}}{u^{1/b}+(1-u)^{1/b}}\right)^{1/a}\right].$$

3.2. Asymptotic Properties

The asymptotics of CDF and PDF when $x \to -\infty$ are

$$F(x) \sim \left(\frac{1}{2}\right)^{ab} e^{abx}, \qquad f(x) \sim ab\left(\frac{1}{2}\right)^{ab} e^{abx}, \tag{3}$$

whereas, when $x \to +\infty$,

$$1-F(x) \sim \left(\frac{a}{2}\right)^{b} e^{-bx}, \qquad f(x) \sim b\left(\frac{a}{2}\right)^{b} e^{-bx}. \tag{4}$$

3.3. Linear Representation

For any δ, we have

$$\begin{aligned}\Pi(x)^{\delta} &= \sum_{n=0}^{\infty}\sum_{j=0}^{n}(-1)^{n+j}\binom{\delta}{n}\binom{n}{j}\Pi(x)^{j}\\ &= \sum_{j=0}^{\infty}\sum_{n=j}^{\infty}(-1)^{n+j}\binom{\delta}{n}\binom{n}{j}\Pi(x)^{j}\\ &= \sum_{j=0}^{\infty}\eta_j\,\Pi(x)^{j},\end{aligned} \tag{5}$$

where

$$\eta_j \equiv \eta_j(\delta) = \sum_{n=j}^{\infty}(-1)^{n+j}\binom{\delta}{n}\binom{n}{j}.$$

Then,

$$\Pi(x)^{a\,b} + [1-\Pi(x)^{a}]^{b} = \sum_{j=0}^{\infty}\alpha_j\,\Pi(x)^{j}, \tag{6}$$

where

$$\alpha_j \equiv \alpha_j(a,b) = \eta_j(a\,b) + \sum_{i=0}^{\infty}(-1)^{i}\binom{b}{i}\eta_j(i\,a).$$

Finally, $F(x)$ comes from the ratio of two power series as

$$F(x) = \sum_{j=0}^{\infty}\psi_j\,\Pi(x)^{j}, \tag{7}$$

where $\psi_0 = \frac{\eta_0}{\alpha_0}$ and, for $j \geq 1$, and

$$\psi_j \equiv \psi_j(a,b) = \frac{1}{\alpha_0}\left(a_j - \frac{1}{\alpha_0}\sum_{r=1}^{j}\eta_r\,\alpha_{j-r}\right).$$

Equation (7) gives the CDF of X as a power series of SLa CDFs. In addition, by simple differentiation, we have that

$$f(x) = \begin{cases}\sum_{j=1}^{\infty}\epsilon_j e^{jx}, & x \leq 0,\\ \sum_{j=1}^{\infty}\sum_{k=0}^{j-1}\rho_{j,k}e^{-(k+1)x}, & x \geq 0,\end{cases} \tag{8}$$

where

$$\epsilon_j = j\left(\frac{1}{2}\right)^{j}\psi_j, \quad \rho_{j,k} = (-1)^{k}j\left(\frac{1}{2}\right)^{k+1}\binom{j-1}{k}\psi_j,$$

depend on both a and b. Equation (8) shows that the PDF of X is just a linear combination of ESLa densities.

3.4. Moments

Theorem 1. *The n-th ordinary moment of $X \sim GOLLSLa(a,b)$ reduces to*

$$E(X^{n}) = (-1)^{n}\,n!\sum_{j=1}^{\infty}\frac{\epsilon_j}{j^{n+1}} + n!\sum_{j=1}^{\infty}\sum_{k=0}^{j-1}\frac{\rho_{j,k}}{(k+1)^{n+1}}, \tag{9}$$

where $\Gamma(a) = \int_0^{\infty} z^{a-1}e^{-z}dz$ is the gamma function.

Proof. Note that

$$\int_{-\infty}^{0} x^n f(x)dx = \sum_{j=1}^{\infty} \epsilon_j \int_{-\infty}^{0} x^n e^{jx} dx$$
$$= (-1)^n n! \sum_{j=1}^{\infty} \frac{\epsilon_j}{j^{n+1}}$$

and

$$\int_{0}^{\infty} x^n f(x)dx = \sum_{j=1}^{\infty} \sum_{k=0}^{j-1} \rho_{j,k} \int_{0}^{\infty} x^n e^{-(k+1)x} dx$$
$$= n! \sum_{j=1}^{\infty} \sum_{k=0}^{j-1} \frac{\rho_{j,k}}{(k+1)^{n+1}}.$$

If $x \leq 0$ as well as $x > 0$, by combining latter results, Theorem 1 is proved. □

Theorem 2. *The n-th order incomplete moment of $X \sim GOLLSLa(a, b)$ (for $y > 0$) is*

$$m_n(y) = \frac{1}{F(y)} \left[\sum_{j=1}^{\infty} \frac{(-1)^n}{j^{n+1}} \epsilon_j \Gamma(n+1, -jy) + \sum_{j=1}^{\infty} \sum_{k=0}^{j-1} \frac{\rho_{j,k} \gamma(n+1, (k+1)y)}{(k+1)^{n+1}} \right], \quad (10)$$

and, for $y < 0$,

$$m_n(y) = \frac{1}{F(y)} \sum_{j=1}^{\infty} \frac{(-1)^n}{j^{n+1}} \epsilon_j \Gamma(n+1, -jy), \quad (11)$$

where $\Gamma(s, w) = \int_w^{\infty} z^{s-1} e^{-z} dz$ is the upper incomplete gamma function, and $\gamma(s, w) = \int_0^w z^{s-1} e^{-z} dz$ is the lower incomplete gamma function.

Proof. The n-th incomplete moment of $X \sim \text{GOLLSLa}(a, b)$ can be expressed as

$$m_n(y) = E[X^n | X < y]$$
$$= \frac{1}{F(y)} \int_{-\infty}^{y} x^n f(x)dx.$$

For $y > 0$, it follows from (8) that

$$\int_{-\infty}^{y} x^n f(x)dx = \sum_{j=1}^{\infty} \epsilon_j \int_{-\infty}^{0} x^n e^{jx} dx + \sum_{j=1}^{\infty} \sum_{k=0}^{j-1} \rho_{j,k} \int_{0}^{y} x^n e^{-(k+1)x} dx,$$

where

$$\int_{-\infty}^{0} x^n e^{jx} dx = (-1)^n n! \frac{1}{j^{n+1}},$$
$$\int_{0}^{y} x^n e^{-(k+1)x} dx = \frac{\gamma(n+1, (k+1)y)}{(k+1)^{n+1}}, \quad y > 0.$$

In a similar manner, for $y < 0$,

$$\int_{-\infty}^{y} x^n f(x)dx = \sum_{j=1}^{\infty} \epsilon_j \int_{-\infty}^{y} x^n e^{jx} dx$$
$$= (-1)^n \sum_{j=1}^{\infty} \frac{\epsilon_j \Gamma(n+1, -jy)}{j^{n+1}},$$

which proves Theorem 2. □

3.5. Quantiles and Pseudo-Random Generator

Property 1. *Let $X \sim GOLLSLa(a, b)$. Consequently, the p-th $(0 < p < 1)$ quantile of X is the solution of*

$$\Pi(x_p)^{ab} - p\left[\Pi(x_p)^{ab} + \left(1 - \Pi(x_p)^a\right)^b\right] = 0. \tag{12}$$

Proof. Equation (12) follows from (1). Suppose $R \sim U(0, 1)$, by setting $p = R$ in (12), the generated variate X is obtained. □

4. Estimation Procedure

The estimation of the proposed distribution is carried out using the maximum likelihood method, which has been extensively studied for parameter inference in flexible and complex distributions under various sampling schemes (see [11] for details). By including a location μ and a scale $\sigma > 0$, the PDF of $Y = (X - \mu)/\sigma \sim$ GOLLSLa(μ, σ, a, b) becomes

$$f(y) = a\, b\, \pi(y; \mu, \sigma)\Pi(y; \mu, \sigma)^{ab-1}[1 - \Pi(y; \mu, \sigma)^a]^{b-1}$$
$$\times \left\{\Pi(y; \mu, \sigma)^{ab} + [1 - \Pi(y; \mu, \sigma)^a]^b\right\}^{-2}, \tag{13}$$

where

$$\pi(y; \mu, \sigma) = (2\sigma)^{-1} \mathrm{e}^{-\left|\frac{y-\mu}{\sigma}\right|},$$
$$\Pi(y; \mu, \sigma) = \frac{1}{2} + \frac{\mathrm{Sign}\left(\frac{y-\mu}{2\sigma}\right)}{2}\left[1 - \mathrm{e}^{-\left|\frac{y-\mu}{\sigma}\right|}\right],$$

and $\mathrm{Sign}(w)$ is -1, 0, or 1 if w is positive, zero, or negative.

Consider independent and identically distributed observations $y_1, \cdots, y_n$ from (13). The log-likelihood function for $\boldsymbol{\theta} = (\mu, \sigma, a, b)$ is

$$l(\boldsymbol{\theta}) = n\log(ab) - \sum_{i=1}^{n}\left|\frac{y_i - \mu}{\sigma}\right| - n\log(2\sigma) + (ab - 1)\sum_{i=1}^{n}\log\Pi(y_i; \mu, \sigma)$$
$$+ (b - 1)\sum_{i=1}^{n}\log\left[1 - \Pi(y_i; \mu, \sigma)^a\right]$$
$$- 2\sum_{i=1}^{n}\log\left[\Pi(y_i; \mu, \sigma)^{ab} + (1 - \Pi(y_i; \mu, \sigma)^a)^b\right]. \tag{14}$$

The maximum likelihood estimate (MLE) $\widehat{\boldsymbol{\theta}}$ can be found by maximizing (14) via the `PROC NLMixed` in SAS (version 9.4) and `AdequacyModel` or `maxLik` libraries from `R` (version 4.3.2) software, or `optim` function from `R` `GenSA` package (version 4.3.2).

Differentiating (14) in relation to the parameters, the likelihood equations can be determined from

$$\frac{\partial l(\theta)}{\partial \mu} = \sum_{i=1}^{n} \frac{a - b\mu + 2}{a^2(D(1)^2)} + \sum_{i=1}^{n} \frac{|y_i - \mu|}{b(D(2) - 3)} - \sum_{i=1}^{n} \frac{3(1-b)}{(1 - D(2))D(3)},$$

$$\frac{\partial l(\theta)}{\partial \sigma} = -\frac{n}{\sigma} + \frac{a}{2\sigma^3} \sum_{i=1}^{n} \frac{(y_i - \mu)^{3/2}}{\sigma} + \sum_{i=1}^{n} \frac{2b(y_i - \mu)(\mu - by_i)}{a^4 D(3)^2} + \sum_{i=1}^{n} \frac{|y_i - \mu|}{b^2},$$

$$\frac{\partial l(\theta)}{\partial a} = \sum_{i=1}^{n} \left(a + be^{D(1)/3}\right)^{-1} + -\frac{n}{a^4} - \sum_{i=1}^{n} \frac{(y_i - aD(1)D(3)^2)}{b^2} + \sum_{i=1}^{n} \frac{b}{a^5} |y_i - \mu|,$$

$$\frac{\partial l(\theta)}{\partial b} = \sum_{i=1}^{n} (D(2) + a)^{-1} - \sum_{i=1}^{n} \frac{y_i - \mu}{2\sigma^2} - \sum_{i=1}^{n} \log\left(\mathrm{e}^{-\frac{y_i - \mu}{\sigma}} + D(3)\right) - 2\sum_{i=1}^{n} \frac{D(3)(\mu - \sigma D(2) - y_i)}{\sigma^2 D(4)^3},$$

where

$$D(1) = \left|\frac{y_i - \mu}{\sigma}\right| + 1,$$
$$D(2) = \mathrm{e}^{\frac{y_i}{\sigma}} + \mathrm{e}^{\mu/\sigma},$$
$$D(3) = \mathrm{e}^{\frac{-b\mu + by_i + \mu}{\sigma}},$$
$$D(4) = D(1)^a + \mathrm{e}^{\frac{(y_i - \mu)b}{\sigma}} D(1).$$

5. Simulation Study

The `GenSA` package of `R` software is utilized to perform the simulation process. The initial estimate for μ is randomly chosen in the interval $\mu_s \in (\mu - 0.25, \mu + 0.25)$. Similarly, for the remaining parameters, the starting values are selected from the range $\boldsymbol{\theta}_s \in (\boldsymbol{\theta} - 0.25, \boldsymbol{\theta} + 0.25)$. The bias and mean square error (MSE) of $\hat{\boldsymbol{\theta}}$ are given by

$$\begin{aligned} \mathrm{Bias}(\hat{\boldsymbol{\theta}}) &= E(\hat{\boldsymbol{\theta}}) - \boldsymbol{\theta}, \\ \mathrm{MSE}(\hat{\boldsymbol{\theta}}) &= V(\hat{\boldsymbol{\theta}}) + \mathrm{Bias}(\hat{\boldsymbol{\theta}})^2. \end{aligned}$$

Here, $\hat{\boldsymbol{\theta}} = (\hat{\mu}, \hat{\sigma}, \hat{a}, \hat{b})$.

We performed 10,000 randomly generated samples for $n = 100, 300, 500$. These samples were drawn from the GOLLSLa distribution with parameters $(0, 1, a, b)$ for some values of a and b. The results of the simulations are reported in Tables 1 and 2. In both tables, a clear improvement in estimation accuracy is observed as the sample size increases from $n = 100$ to $n = 500$, with the MSE values decreasing for all parameters, which confirms the consistency of the MLEs. The bias values of μ and σ remain relatively small and tend to fluctuate around zero for larger samples, indicating stable estimation of the location and scale parameters. Comparing Table 1 ($a = 2$) and Table 2 ($a = 4$), similar convergence patterns are observed, suggesting that the estimation procedure is robust across different levels of model skewness and tail behavior. Overall, the Tables show that the MLEs are consistent because they tend to the true parameters as n increases.

Table 1. Simulation results for $a = 2$.

			$\mu = 0, \quad \sigma = 1$							
			μ		σ		a		b	
a	b	n	**Bias**	**MSE**	**Bias**	**MSE**	**Bias**	**MSE**	**Bias**	**MSE**
		100	0.2661	0.0839	−0.3177	0.2811	−0.2171	0.1821	0.5881	0.3812
	0.5	300	−0.2301	0.0822	0.3022	0.2751	0.2011	0.1799	−0.5561	0.3721
		500	0.2230	0.0724	0.2998	0.2700	0.1982	0.1702	−0.5002	0.3555
		100	0.4377	0.3717	0.2711	0.1661	0.5196	0.2188	0.3771	0.2861
	1.5	300	−0.4510	0.3291	−0.2514	0.0951	0.5000	0.2016	−0.3266	0.2716
		500	−0.4422	0.3199	−0.2291	0.0866	0.4765	0.1991	0.3018	0.2444
		100	−0.4403	0.0683	0.4320	0.3101	0.4363	0.2349	0.4004	0.2329
2	2.5	300	−0.4109	0.2030	−0.0281	0.0065	−0.3016	0.1241	−0.3495	0.2009
		500	−0.4029	0.2006	−0.0083	0.0026	−0.3010	0.1111	−0.2905	0.1654
		100	0.2112	0.0411	−0.1139	0.0311	−0.3343	0.0239	−0.2378	0.0976
	3.5	300	0.2011	0.0235	0.0987	0.0265	−0.2898	0.0129	0.2199	0.0154
		500	−0.1240	0.0196	−0.0744	0.0211	−0.3122	0.0101	0.1184	0.0072
		100	0.3714	0.2881	0.4811	0.3816	−0.1772	0.0911	0.3221	0.2210
	4.5	300	−0.3000	0.2510	−0.4221	0.2371	0.1661	0.0844	0.2891	0.1988
		500	0.2767	0.2281	0.3711	0.1642	0.1001	0.0711	0.2511	0.1777

Table 2. Simulation results for $a = 4$.

			$\mu = 0, \quad \sigma = 1$							
			μ		σ		a		b	
a	b	n	**Bias**	**MSE**	**Bias**	**MSE**	**Bias**	**MSE**	**Bias**	**MSE**
		100	0.0317	0.1441	0.0551	0.2816	0.2551	0.2251	−0.6131	0.3117
	0.5	300	−0.0215	0.1211	0.0418	0.1532	−0.2331	0.1341	−0.3441	0.2441
		500	0.0211	0.1101	0.0318	0.1173	−0.1781	0.1110	0.4155	0.3188
		100	0.2117	0.0415	0.4412	0.3515	0.1771	0.0922	−0.1551	0.3711
	1.5	300	−0.1232	0.0255	0.3441	0.2551	−0.1591	0.0613	0.1900	0.3901
		500	−0.1011	0.0200	−0.2551	0.1983	0.1491	0.0551	0.1601	0.3081
		100	0.0981	0.0281	−0.1465	0.0610	0.3318	0.6133	−0.2331	0.0923
4	2.5	300	0.0825	0.0189	0.1287	0.0418	−0.2431	0.5834	0.2014	0.0681
		500	0.0510	0.0200	0.1149	0.0211	0.2220	0.5006	0.1862	0.0491
		100	0.0441	0.0414	−0.4551	0.0359	−0.1349	0.0261	−0.6123	0.4519
	3.5	300	−0.0319	0.0400	0.3911	0.0316	0.1258	0.0258	0.6013	0.4444
		500	0.0198	0.0371	0.3011	0.0291	0.1198	0.0178	0.5198	0.3819
		100	−0.0341	0.1159	−0.1811	0.0931	−0.5182	0.3177	−0.0938	0.0235
	4.5	300	0.0316	0.0900	0.1513	0.0710	0.4916	0.3001	0.0834	0.0211
		500	0.0291	0.0712	0.0853	0.0707	0.4711	0.2881	−0.0816	0.0111

6. Applications

The flexibility of the new distribution is compared with the standard normal (N), La, the skew normal (SN) [1], SLa [12], $OLLSLa$, and $ESLa$ (see Remark 1) through the Akaike Information Criterion (AIC) and the Bayesian Information Criterion (BIC).

6.1. BMI Data

The BMI of 202 Australian athletes was considered here [13]. The MLEs, maximum log-likelihoods, AIC, and BIC values for the fitted models are shown in Table 3.

Table 3. Fitted model results to BMI data.

Distribution	$\hat{\mu}$	$\hat{\sigma}$	$\hat{a}$	$\hat{b}$	$\hat{\lambda}$	log L	AIC	BIC
N	22.956	2.857	—	—	—	−498.668	1001.336	1007.953
La	22.749	2.123	—	—	—	−494.080	992.160	998.776
SN	19.969	4.133	—	—	2.313	−490.099	986.198	996.123
SLa	22.350	2.084	—	—	0.865	−492.461	990.922	1000.847
OLLSLa	22.759	24.27	—	8.522	—	−490.941	987.882	997.806
ESLa	21.200	2.532	1.931	—	—	−491.026	988.051	997.976
GOLLSLa	16.750	6.469	3.106	2.701	—	−486.704	981.408	994.641

Table 3 shows that the new distribution is more suitable than other competitors for these data. Figure 3 illustrates its flexibility.

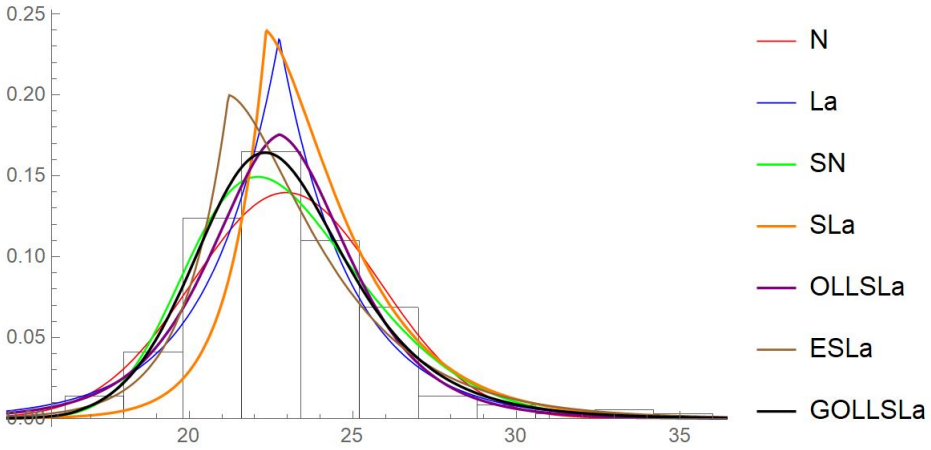

Figure 3. Observed and expected densities for BMI data.

6.2. Enzyme Data

This analysis considers 245 enzyme observations analyzed by [14]. Table 4 reports the MLEs, maximum log-likelihoods, and the AIC and BIC values for the fitted models.

Table 4. Fitted model results for enzyme data.

Distribution	$\hat{\mu}$	$\hat{\sigma}$	$\hat{a}$	$\hat{b}$	$\hat{\lambda}$	log L	AIC	BIC
N	0.622	0.621	—	—	—	−230.761	465.522	472.525
La	0.264	0.460	—	—	—	−224.815	453.630	460.632
SN	0.039	0.851	—	—	40.777	−142.115	290.230	300.733
SLa	0.558	0.065	—	—	29.467	−114.013	234.026	244.529
OLLSLa	0.230	0.232	—	0.535	—	−221.572	449.144	459.647
ESLa	0.108	0.436	2.788	—	—	−163.920	333.840	344.343
GOLLSLa	0.128	0.085	20.84	0.138	—	−69.7441	147.488	161.493

The appropriateness of the new distribution is clearly evident from Table 4 with regard to the values of model selection criterion. Figure 4 also shows the adaptability of the new distribution.

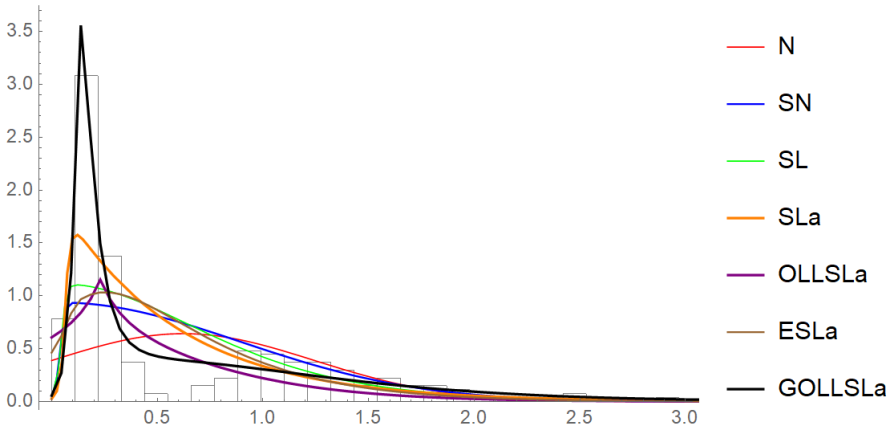

Figure 4. Observed and expected densities for enzyme data.

7. Hypothesis Tests

We adopt likelihood ratio (LR) (for more details see [15,16]) statistics to compare nested models as follows.

(i) For testing La versus GOLLSLa, the LR statistic is

$$w = -2[\log L(\hat{\mu}_1, \hat{\sigma}_1, a = b = 0|x) - \log L(\hat{\mu}_2, \hat{\sigma}_2, \hat{a}_2, \hat{b}_2)],$$

where $(\hat{\mu}_1, \hat{\sigma}_1)$ and $(\hat{\mu}_2, \hat{\sigma}_2, \hat{a}_2, \hat{b}_2)$ are the MLEs of the La and GOLLSLa models, respectively.

(ii) For testing OLLSLa versus GOLLSLa,

$$w = -2[\log L(\hat{\mu}_1, \hat{\sigma}_1, \hat{b}_1, a = 1|x) - \log L(\hat{\mu}_2, \hat{\sigma}_2, \hat{a}_2, \hat{b}_2)],$$

where $(\hat{\mu}_1, \hat{\sigma}_1, \hat{b}_1)$ and $(\hat{\mu}_2, \hat{\sigma}_2, \hat{a}_2, \hat{b}_2)$ are the MLEs of the OLLSLa and GOLLSLa distributions, respectively.

(iii) For testing ESLa versus GOLLSLa,

$$w = -2[\log L(\hat{\mu}_1, \hat{\sigma}_1, \hat{a}_1, b = 1|x) - \log L(\hat{\mu}_2, \hat{\sigma}_2, \hat{a}_2, \hat{b}_2)],$$

where $(\hat{\mu}_1, \hat{\sigma}_1, \hat{a}_1)$ and $(\hat{\mu}_2, \hat{\sigma}_2, \hat{a}_2, \hat{b}_2)$ are the MLEs of the ESLa and GOLLSLa distributions, respectively.

In cases (ii) and (iii), the null hypotheses are composite, since parameters other than the one being tested are estimated under both the null and alternative models. However, the corresponding submodels (OLLSLa and ESLa) are nested within the full GOLLSLa model by fixing $a = 1$ or $b = 1$, respectively. Hence, the likelihood ratio statistic involves one restriction and follows asymptotically a χ^2 distribution. Table 5 shows that the GOLLSLa(μ, σ, a, b) distribution is more appropriate for both datasets.

Table 5. LR tests for BMI and Enzyme datasets.

Hypotheses	LR Statistic		df	Critical Value at 5%
	BMI	Enzyme		
$H_0 : a = 0, b = 0$ vs. $H_1 : a \neq 0, b \neq 0$	14.752	310.142	2	5.991
$H_0 : a = 1$ vs. $H_1 : a \neq 1$	8.474	151.831	1	3.841
$H_0 : b = 1$ vs. $H_1 : b \neq 1$	8.644	94.179	1	3.841

8. Risk Analysis

The MO^P, VaR$[q]$ and PORT-VaR$[q]$ methods are essential tools for evaluating the BMI measurements of Australian athletes; see [5,17,18]. These methods equip investors and policymakers with the tools needed for informed decision-making and contribute to building a more resilient real estate market; see [19,20]. For a comprehensive theoretical treatment of statistical estimation procedures for Value-at-Risk and related risk measures, we refer the reader to see [21].

8.1. MO^P

As highlighted in [20,22], varying the $\mathrm{MO}^{\{P\}}$ (mean of order P) provides a powerful tool to conduct a deeper and more comprehensive analysis of data distributions, particularly in the context of financial risk assessment and modeling. It enables the examination of different aspects of data, including central tendencies and tail behaviors, by adjusting the order parameter PP. This adaptability allows researchers to tailor their analysis to the specific features of the dataset, such as focusing on extreme values or capturing subtle variations in the distribution. The $\mathrm{MO}^{\{P\}}$ is given by

$$\mathrm{MO}^{\{P\}} = \left(\frac{1}{n} \sum_{i=1}^{n} x_i^P \right)^{\frac{1}{P}}.$$

8.2. VaR$[q]$

The value x is the VaR at a confidence level q if $\Pr(X \leq x) = q$. Equation $F(x) = q$ must be solved for this. The positive portion of $F(x)$ is utilized for values of $x \geq 0$.

8.3. PORT-VaR$[q]$

Refs. [23,24] reported that the PORT-VaR approach is a very important technique in risk analysis. Its foundation is the conventional VaR method. Nonetheless, the PORT-VaR approach encourages better decisions in risk analysis; see [20].

8.4. Risk Analysis for the BMI Dataset

The risk analysis for BMI measurements of Australian athletes reported in Table 6 highlights important trends but requires further clarification to maximize its impact. The decreasing Bias and MSE when P increases indicate that higher-order models improve accuracy and reduce errors, potentially offering more reliable predictions. However, the significance of $P \uparrow$ increases, TMV, and $\mathrm{MO}^{\{P\}}$ should be clearly defined to enhance interpretability for readers unfamiliar with the methodology. Alternatively, Figure 5 displays the Cullen–Frey analysis (top left), the Kernel Density Estimation (KDE) (top right), the Violin plot (bottom left), and the QQ plot (bottom right) for these measurements. The Cullen–Frey plot reveals that the median BMI values do not follow any standard distribution, indicating that factors outside traditional models may be influencing these measurements. Conversely, the KDE (top right) offers a smooth representation of the distribution, shedding light on the underlying PDF and highlighting patterns and trends that may not be immediately visible in the raw data. The Violin plot illustrates the 1st quartile, median, and 3rd quartile for the BMI measurements. Lastly, the QQ plot highlights the extreme values in the data, showcasing potential outliers or deviations.

While the analysis is specific to Australian athletes, its applicability to broader populations remains unclear, warranting a discussion of demographic differences. The consistent reduction in Bias implies that systematic errors are mitigated as model complexity increases, which could enhance the precision of BMI-related risk assessments. Additionally, the sharp decline in MSE indicates better prediction reliability at higher orders of P. These

findings are promising but require a connection to practical health implications, such as identifying BMI thresholds that signify risk for obesity or underweight conditions. Table 6 could benefit from visual aids like graphs to emphasize key trends, making the data more accessible. Furthermore, the limitations of the dataset, such as sample size or the absence of confounding factors like age, gender, or type of sport, should be acknowledged. Based on this table, we conclude:

(1) The $MO^{\{P\}}$ provides a progression across varying "P" values. However, the practical significance of this analysis in terms of BMI risk factor deserves to be explained. For example, how does a change in P from 1 to 15 impact the interpretation of BMI trends among Australian athletes?
(2) Bias consistently decreases as "$P \uparrow$" increases, suggesting a potential reduction in systematic error. This trend may indicate that higher order-P values are more reliable for BMI risk assessments. The implications of this decreasing bias in terms of health risk predictions should be addressed explicitly.
(3) The Mean Squared Error (MSE) decreases significantly with increasing "P" from 38.51 at $P = 1$ to 21.52 at $P = 15$. This suggests that higher-order models might provide better predictions. Linking this finding to some BMI-related risks (e.g., obesity, underweight) would enhance the analysis.
(4) The main recommendation from Table 6 is to prioritize higher-order models (e.g., $P = 10$ or $P = 15$) for BMI measurements when assessing risks for Australian athletes. These models exhibit lower Bias and significantly reduced MSE compared to lower-order models, indicating improved accuracy and reliability. Implementing these higher-order models can enhance the identification of BMI-related health risks, such as obesity or underweight conditions, allowing for more precise and effective interventions. However, further validation with diverse populations and consideration of additional factors (e.g., age, gender, and type of sport) is advised to generalize these findings and refine their practical applications.
(5) Table 6 underscores the importance of selecting appropriate order P values to strengthen PORT-based analysis, ensuring that BMI-related health risks are assessed with higher precision and reliability.

Table 6. $MOO_{[P\uparrow]}$ assessment ($P = 1, \ldots, 25$) for the BMI measurements.

$P\uparrow$ |TMV	1	2	3	4	5	10	15
TMV				22.95589			
MO^P	16.75	16.9	16.95333	17.1	17.238	17.78222	18.31667
MSE	38.51308	36.67382	36.0307	34.29146	32.69428	25.56203	21.5224
Bias	6.205891	6.055891	6.002558	5.855891	5.717891	5.055891	4.639224

By analyzing interplay among Bias, MSE, and $MO^{\{P\}}$, Table 6 supports the selection of optimal P values (e.g., $P = 10$ or $P = 15$) to enhance the reliability of the PORT-based analysis. It brings error reduction and bias correction directly translating into improved accuracy in detecting BMI values that exceed risk thresholds, making it an important tool for targeted health interventions.

Table 7 reports an analysis of VaR, PORT-$MO^{\{P\}}$, and the number of PORTs (NPORTs) for BMI data at some Confidence Levels (CLs). The table also summarizes some key statistical metrics of the BMI data. The VaR decreases if CL increases. For example, at 55% CL, VaR is 22.449, while at 95% CL, it drops to 19.003. This suggests that as the level of certainty rises, the threshold for acceptable risk becomes more conservative. It rises from 23.0920 at 55% CL to 27.5515 at 95% CL, indicating that the average losses in the tail of the distribution become more significant at higher CLs. The PORT-$MO^{\{P\}}$

values, for portfolio risk, fluctuate slightly but remain generally consistent across CLs. The values range from 2.0072 at 80% CL to 2.9012 at 95% CL, suggesting an increasing risk exposure as CLs become higher. The NPORTs increase steadily with higher CLs, from 111 at 55% CL to 191 at 95% CL. This growth shows that larger portions of the data are taken when CLs rise. The minimum value remains constant across all CLs at approximately 19.06, while the maximum remains fixed at 34.42. The interquartile range (1st quartile to 3rd quartile) and median decrease slightly as the CL increases, suggesting a shift in the data central tendency as more extreme values are factored in. This table provides crucial insights into the risk characteristics of BMI measurements. The decreasing VaR at higher confidence levels highlights the importance of considering tail risk, especially when evaluating extreme outcomes. The relatively stable PORT-MO$^{\{P\}}$ values indicate a manageable portfolio risk profile across confidence levels, although the rise in NPORT suggests a broader scope of risk assessment as more conservative thresholds are applied. The statistical summary (e.g., quartiles and median) provides a granular view of the BMI distribution, showing how variations in data become more pronounced under stricter conditions. Overall, these findings are essential to understand the underlying risks and distribution patterns, potentially aiding in the development of strategies for managing BMI-related health metrics or extending this methodology to other domains such as housing markets or financial risks.

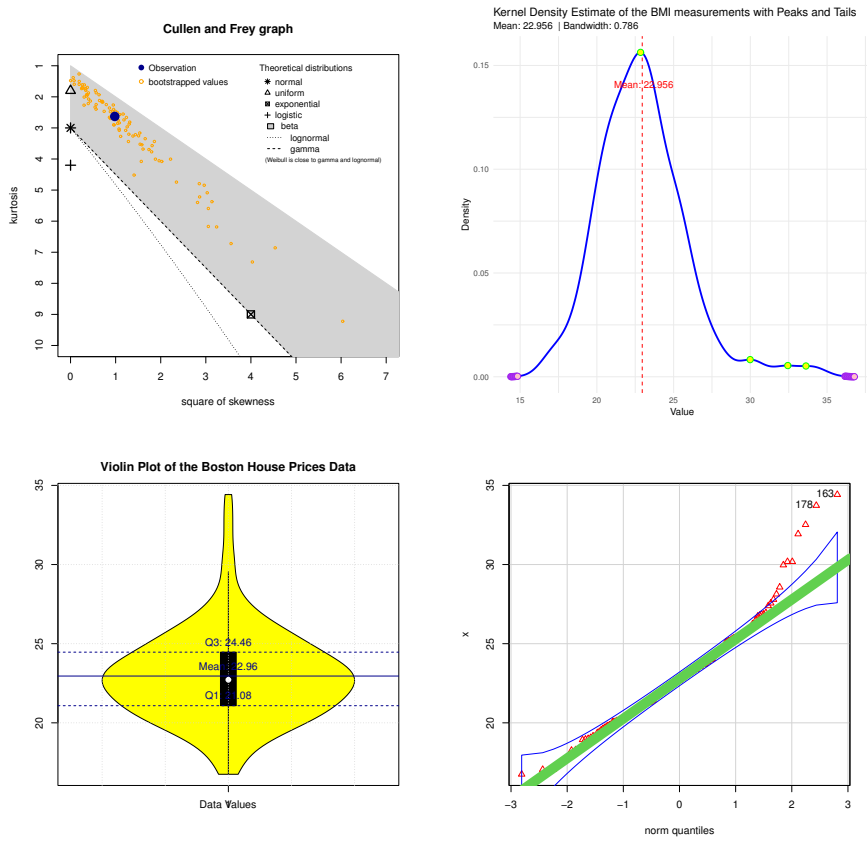

Figure 5. (**Left**) Cullen–Frey graph based on sample skewness and kurtosis, including observed values and bootstrap replications. (**Top right**) Kernel density estimate of the BMI measurements, where the solid blue curve represents the estimated density, the red dashed vertical line denotes the sample mean, and the colored points highlight the distributional behavior in the tails. (**Bottom left**) Violin plot of the BMI data showing the empirical distribution, median, and quartiles. (**Bottom right**) Quantile–quantile (Q–Q) plot comparing empirical quantiles with theoretical normal quantiles; the solid line indicates the reference line, and the curved bands represent pointwise confidence envelopes.

A frequency distribution of median BMI values for nine CLs is shown in nine histograms in Figure 6. Analysts may see how frequently particular failure time ranges happened over the research period due to this comparison graphic. Understanding trends and abnormalities that can have an impact on investment strategy and market stability requires these kinds of observations. A density plot of peaks at different thresholds is shown in Figure 7, highlighting the distribution and frequency of important events in the data. Because it allows analysts to evaluate the possibility of severe swings, which can have a significant influence on investment decisions and economic stability, this visualization is essential for risk assessment. PORT study of median BMI data using violin plots is shown in Figure 8. These diagrams provide a good understanding of the risk profiles associated with housing investments, also highlighting the median and interquartile ranges and providing light on the density of data at various levels. Figures 5–8 reinforce the numerical findings outlined in Table 7, thus providing robust support for our findings.

Table 7. Statistical outcomes for BMI data.

CLs↓	VaR	T_h	PORT-MO^P	NPORT	Min.; 1st Qu.; Med; ExV; 3rd Qu.; Max.
55%	22.449	23.0920	2.2242	111	22.46; 23.27; 24.21; 24.86; 25.55 34.42
60%	22.124	23.3340	2.2438	121	22.13; 23.11; 23.97; 24.65; 25.43; 34.42
65%	21.860	23.6385	2.2350	129	21.88; 22.93; 23.84; 24.48; 25.37; 34.42
70%	21.359	23.9700	2.2850	141	21.38; 22.63; 23.67; 24.24; 25.27; 34.42
75%	21.083	24.4650	2.1558	151	21.12; 22.39; 23.55; 24.04; 25.17; 34.42
80%	20.674	25.0840	2.0072	161	20.69; 22.13; 23.35; 23.85; 25.09; 34.42
85%	20.189	25.4225	2.2646	171	20.30; 21.89; 23.19; 23.65; 24.87; 34.42
90%	19.814	26.0560	2.5926	181	19.85; 21.68; 23.11; 23.45; 24.64; 34.42
95%	19.003	27.5515	2.9012	191	19.06; 21.27; 22.96; 23.24; 24.54; 34.42

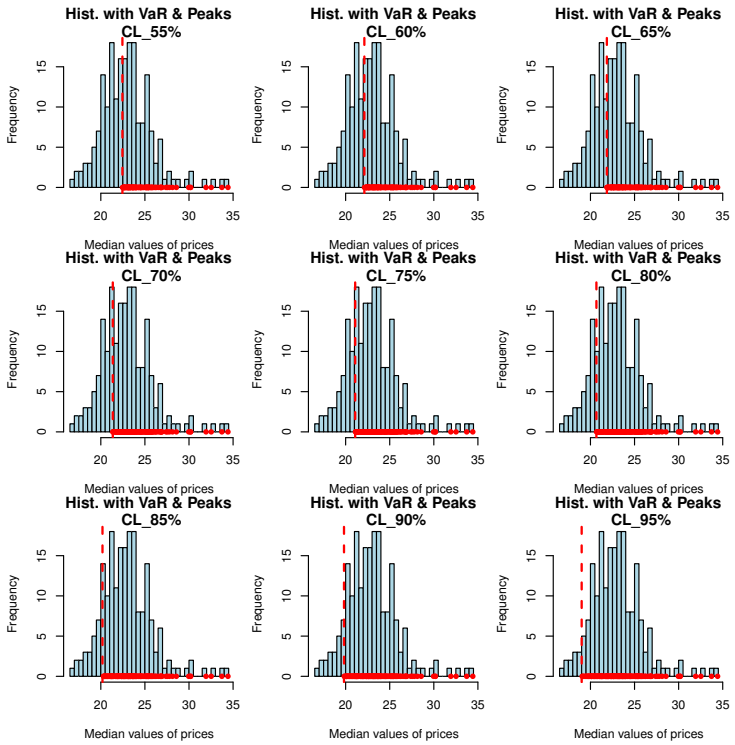

Figure 6. PORT-VaR analysis of median BMI values at different confidence levels. The red dotted vertical line indicates the VaR threshold, while the red horizontal segment highlights the peak region of the empirical distribution.

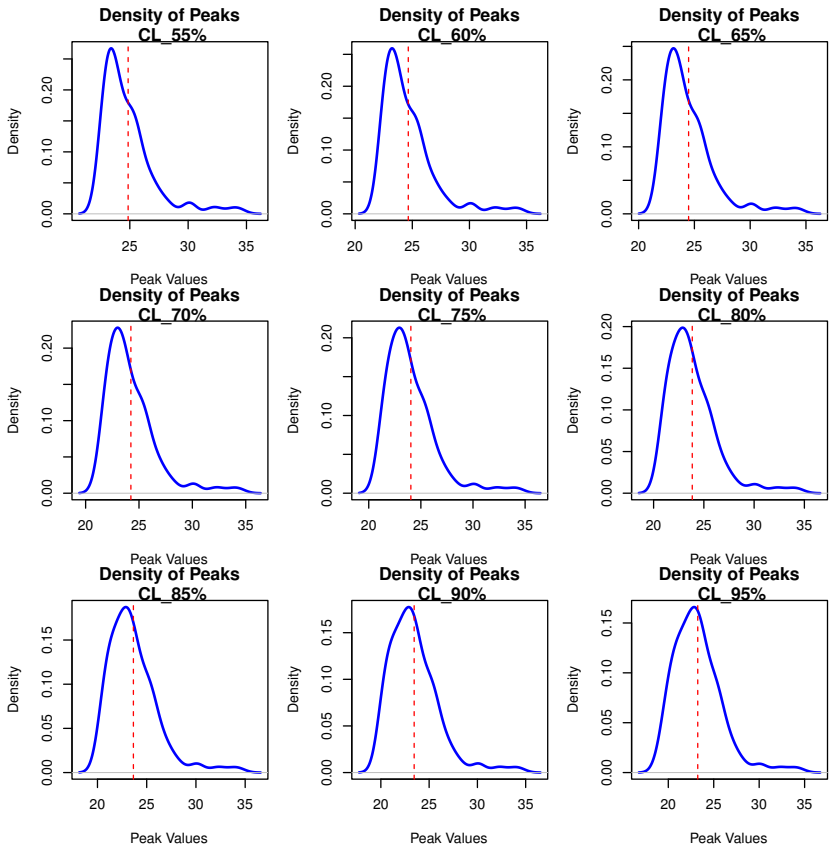

Figure 7. Graphs of density of peaks exceeding the medians in BMI data. The red dotted vertical line denotes the PORT-VaR threshold.

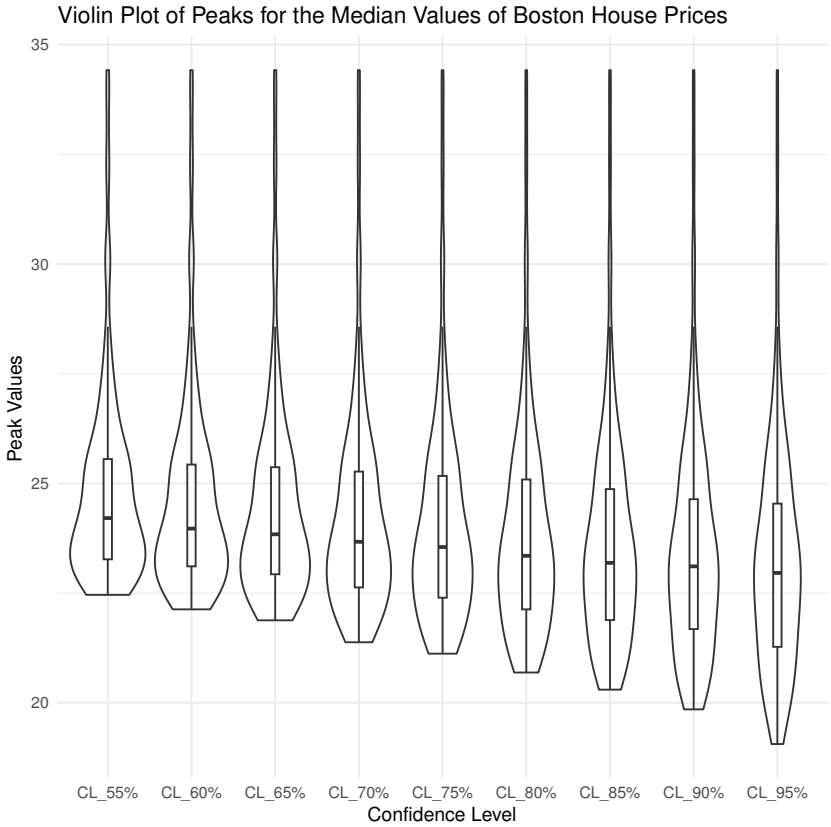

Figure 8. Graphs of Violin plots for the PORT analysis of medians in BMI data.

Table 7 provides vital information for the BMI measurements of Australian athletes, which are crucial to monitoring and improving their health. These data allow medical professionals to identify individuals at risk and implement personalized interventions. Furthermore, understanding the variability and risk factors associated with BMI can inform the design of targeted health initiatives aimed at maintaining optimal fitness levels in athletes, reducing the risk of injuries and enhancing their long-term health outcomes. In the realm of sports, this analysis is instrumental in optimizing athletic performance and ensuring the physical well-being of athletes. BMI is often associated with an athlete's performance, influencing attributes such as speed, endurance, and strength. The table helps sports scientists and coaches identify ideal BMI ranges for different sports and tailor training and nutrition programs accordingly.

Furthermore, analyzing extreme BMI values can help mitigate risk of injury, as athletes with atypical BMI values may be more prone to joint stress, reduced recovery rates, or fatigue. Using such data, stakeholders can set benchmarks and create performance-enhancing strategies while maintaining athletes' physical health and competitive edge. The financial relevance of Table 7 lies in its methodological application to risk analysis and management, concepts that are essential in sectors such as health insurance and investment. Metrics such as VaR originally designed for financial risk assessment, are applied here to identify and quantify extreme BMI values. For health insurers, this dataset is invaluable in estimating potential costs associated with health risks and tailoring insurance premiums. Similarly, organizations that invest in athlete development can take advantage of this information to allocate resources effectively, focusing on areas that produce the highest returns in terms of performance and longevity. Beyond sports, the statistical tools in Table 7 can also be adapted to model risks in financial systems, proving the broader applicability of this approach.

9. Concluding Remarks

In order to improve the current statistical framework and more accurately represent real-life situations, this article presents an extended Laplace distribution. It provides some characteristics, highlighting its unique qualities and benefits over conventional methods. To demonstrate its practical value, a new distribution is applied to real-world datasets, highlighting its versatility across various applications. Using some well-known metrics, a new model is used for a thorough economic risk assessment. These measurements, which are especially useful for analyzing body mass index (BMI) data, capture several facts of tail behavior and provide important insights into high values. The proposed risk analysis can serve as a powerful, multidisciplinary tool, uniting health, sports, and finance through its detailed examination of BMI measurements among Australian athletes. By leveraging these risk metrics, the analysis provides valuable insights for BMI data and their extreme values. This enables the identification of potential health risks, targeted interventions, and optimized strategies to maintain physical fitness and mitigate vulnerabilities. Through its multifaceted approach, this study highlights the utility of advanced statistical models in different fields.

Author Contributions: Conceptualization, M.A. and G.M.C.; methodology, G.M.C., P.J.H. and J.D.; software, P.J.H. and J.D.; validation, J.D. and P.J.H.; formal analysis, J.D. and G.M.C.; investigation, M.A., J.D. and P.J.H.; resources, J.E.C.-R.; data curation, J.D.; writing—original draft preparation, P.J.H., J.D.and H.M.Y.; writing—review and editing, G.M.C., J.E.C.-R., M.S.H. and H.M.Y.; visualization, J.D. and P.J.H.; supervision, M.A., P.J.H. and G.M.C.; project administration, P.J.H. and M.A.; funding acquisition, J.E.C.-R., M.A. and H.M.Y. All authors have read and agreed to the published version of the manuscript.

Funding: This research received no external funding.

Data Availability Statement: The data used in this work are available in the `R 4.5.2` software (https://www.r-project.org/, accessed on 31 October 2025).

Conflicts of Interest: The authors declare that they have no known competing financial interest or conflict of interest that could have appeared to influence the work reported in this paper.

References

1. Azzalini, A. A class of distributions which includes the normal ones. *Scand. J. Stat.* **1985**, *12*, 171–178.
2. Aryal, G.R. Study of Laplace and Related Probability Distributions and Their Applications. Ph.D. Thesis, University of Nebraska-Lincoln, Lincoln, NE, USA, 2006.
3. Longin, F. The threshold effect in expected utility and mean-variance analysis: Results from a medium-term asset allocation. *J. Bank. Financ.* **2005**, *29*, 509–532.
4. Furman, E.; Landsman, Z. Tail variance premium with applications for elliptical portfolio of risks. *ASTIN Bull. J. IAA* **2006**, *36*, 433–462. [CrossRef]
5. Landsman, Z. On the tail mean–variance optimal portfolio selection. *Insur. Math. Econ.* **2010**, *46*, 547–553. [CrossRef]
6. Ibrahim, M.; Emam, W.; Tashkandy, Y.; Ali, M.M.; Yousof, H.M. Bayesian and Non-Bayesian Risk Analysis and Assessment under Left-Skewed Insurance Data and a Novel Compound Reciprocal Rayleigh Extension. *Mathematics* **2023**, *11*, 1593. [CrossRef]
7. Elbatal, I.; Diab, L.S.; Ghorbal, A.B.; Yousof, H.M.; Elgarhy, M.; Ali, E.I. A new losses (revenues) probability model with entropy analysis, applications and case studies for value-at-risk modeling and mean of order-P analysis. *AIMS Math.* **2024**, *9*, 7169–7211. [CrossRef]
8. Tran, T.; Wiskow, C.; Aziz, M.A. Skewed and Flexible Skewed Distributions: A Modern Look at the Distribution of BMI. *Am. J. Undergrad. Res.* **2017**, *14*, 45–64. [CrossRef]
9. Taylor, J.W. Forecasting Value at Risk and Expected Shortfall Using a Semiparametric Approach Based on the Asymmetric Laplace Distribution. *J. Bus. Econ. Stat.* **2019**, *37*, 121–133. [CrossRef]
10. Cordeiro, G.M.; Alizadeh, M.; Ozel, G.; Hosseini, B.; Ortega, E.M.M.; Altun, E. The generalized odd log-logistic family of distributions: Properties, regression models and applications. *J. Stat. Comput. Simul.* **2017**, *87*, 908–932. [CrossRef]
11. Peng, K.; Chen, W. Maximum likelihood estimators and properties of the parameters of the Power Ailamujia distribution under ranked set sampling. *J. Stat. Comput. Simul.* **2025**, *95*, 3705–3727. [CrossRef]
12. Aryal, G.; Nadarajah, S. On the skew Laplace distribution. *J. Inf. Optim. Sci.* **2005**, *26*, 205–217. [CrossRef]
13. Cook, R.D.; Weisberg, S. *An Introduction to Regression Graphics*; Wiley: New York, NY, USA, 1994.
14. Bechtel, Y.C.; Bonaiti-Pellie, C.; Poisson, N.; Magnette, J.; Bechtel, P.R. A population and family study N-acetyltransferase using caffeine urinary metabolites. *Clin. Pharmacol. Ther.* **1993**, *54*, 134–141. [CrossRef] [PubMed]
15. Wilks, S.S. The large-sample distribution of the likelihood ratio for testing composite hypotheses. *Ann. Math. Stat.* **1938**, *9*, 60–62. [CrossRef]
16. Casella, G.; Berger, R.L. *Statistical Inference*, 2nd ed.; Duxbury: Pacific Grove, CA, USA, 2002.
17. McNeil, A.J.; Saladin, T. The Peaks Over Thresholds Method for Estimating High Quantiles of Loss Distributions. In Proceedings of the 28th International ASTIN Colloquium, Cairns, Australia, 13–15 August 1997; Volume 23, p. 43.
18. Klugman, S.A.; Panjer, H.H.; Willmot, G.E. *Loss Models: From Data to Decisions*; John Wiley & Sons: Hoboken, NJ, USA, 2012; Volume 715.
19. Shrahili, M.; Elbatal, I.; Yousof, H.M. Asymmetric Density for Risk Claim Size Data: Prediction and Bimodal Data Applications. *Symmetry* **2021**, *13*, 2357. [CrossRef]
20. Aljadani, A.; Mansour, M.M.; Yousof, H.M. A Novel Model for Finance and Reliability Applications: Theory, Practices and Financial Peaks Over a Random Threshold Value-at-Risk Analysis. *Pak. J. Stat. Oper. Res.* **2024**, *20*, 489–515. [CrossRef]
21. Ridder, T. Basics of statistical VaR-estimation. In *Proceedings of the Risk Measurement, Econometrics and Neural Networks: Selected Articles of the 6th Econometric-Workshop in Karlsruhe, Germany*; Springer: Berlin/Heidelberg, Germany, 1998; pp. 161–187.
22. Yousof, H.M.; Aljadani, A.; Mansour, M.M.; Abd Elrazik, E.M. A New Pareto Model: Risk Application, Reliability MOOP and PORT Value-at-Risk Analysis. *Pak. J. Stat. Oper. Res.* **2024**, *20*, 383–407. [CrossRef]
23. Figueiredo, F.; Gomes, M.I.; Henriques-Rodrigues, L. Value-at-risk estimation and the PORT mean-of-order-p methodology. *REVSTAT-Stat. J.* **2017**, *15*, 187–204.
24. Mohamed, H.S.; Cordeiro, G.M.; Minkah, R.; Yousof, H.M.; Ibrahim, M. A size-of-loss model for the negatively skewed insurance claims data: Applications, risk analysis using different methods and statistical forecasting. *J. Appl. Stat.* **2024**, *51*, 348–369. [CrossRef] [PubMed]

Disclaimer/Publisher's Note: The statements, opinions and data contained in all publications are solely those of the individual author(s) and contributor(s) and not of MDPI and/or the editor(s). MDPI and/or the editor(s) disclaim responsibility for any injury to people or property resulting from any ideas, methods, instructions or products referred to in the content.